Title

Satellite NO2 trends reveal pervasive impacts of wildfire and soil emissions across California landscapes

Journal

Environmental Research Letters, 18(9)

ISSN

1748-9318

Authors

Wang, Yurun
Faloona, Ian C
Houlton, Benjamin Z

Publication Date

2023-09-01

DOI

10.1088/1748-9326/acec5f

Peer reviewed

ENVIRONMENTAL RESEARCH
LETTERS

LETTER

Satellite NO_2 trends reveal pervasive impacts of wildfire and soil emissions across California landscapes

Yurun Wang[1], Ian C Faloona[1,2,*] and Benjamin Z Houlton[3]

[1] Department of Land, Air, and Water Resources, University of California, Davis, CA, United States of America
[2] Air Quality Research Center, University of California, Davis, CA, United States of America
[3] Department of Ecology and Evolutionary Biology and Department of Global Development, Cornell University, Ithaca, NY, United States of America
[*] Author to whom any correspondence should be addressed.

E-mail: icfaloona@ucdavis.edu

Keywords: nitrogen dioxide, soil emissions, wildfires emissions, secular trends, air quality

Supplementary material for this article is available online

OPEN ACCESS

RECEIVED
27 May 2023

REVISED
19 July 2023

ACCEPTED FOR PUBLICATION
1 August 2023

PUBLISHED
29 August 2023

Abstract

Nitrogen dioxide (NO_2) plays a pivotal role in the production of secondary pollutants, most importantly ozone (O_3) and particulate matter. Regulatory controls have greatly reduced NO_2 in cities, where most of the surface monitoring occurs, but the change in rural environments is less certain. Here, we present summertime (June–September) spatio-temporal patterns of NO_2 concentrations using satellite and ground observations across California from 2009–2020, quantifying the differences in NO_2 trends for five distinct land cover classes: urban, forests, croplands, scrublands (shrublands, savannas, and grasslands), and barren (minimally vegetated) lands. Over urban environments, NO_2 columns exhibited continued but weakening downward trends ($-3.7 \pm 0.3\%a^{-1}$), which agree fairly well with contemporaneous trends estimated from the surface air quality network ($-4.5 \pm 0.5\%a^{-1}$). In rural (i.e., non-urban) parts of the state, however, secular trends are insignificant ($0.0–0.4 \pm 0.4\%a^{-1}$) or in the case of remote forests are rapidly on the rise ($+4.2 \pm 1.2\%a^{-1}$). Sorting the NO_2 columns by air temperature and soil moisture reveals relationships that are commensurate with extant parameterizations but do indicate a stronger temperature dependence. We further find that rapidly rising temperatures and, to a lesser extent, decreasing precipitation in response to climate change are acting to increase soil NO_x emissions, explaining about one-third of the observed NO_2 rise in non-urban regions across California. Finally, we show that these trends, or their absence, can be attributed predominantly to the dramatic rise in wildfire frequency, especially since the turn of the 21st century.

1. Introduction

Nitrogen oxides ($NO_x = NO + NO_2$) serve as important precursors to tropospheric ozone (O_3) and fine particulate matter ($PM_{2.5}$) with consequent adverse effects including premature death [1], cardiovascular mortality [2], respiratory diseases [3], and agricultural productivity losses [4]. The primary sources of NO_x involve the thermogenic release during high-temperature combustion in air from vehicles [5] and power plants [6], lightning [7], biomass burning [8], and microbial emissions from soils [9]. A recent modeling study by Silvern *et al* [10] for the continental US (CONUS) estimates the proportion of total emissions from anthropogenic fossil fuel combustion to be only 42% in 2017 and falling. Nitrogen dioxide (NO_2) is a reactive gas with a daytime lifetime of a few hours with respect to its reaction with the hydroxyl radical (OH) [11], and can be observed from space due to its unique absorption spectra [12]. A number of satellites have been deployed to monitor the tropospheric NO_2 vertical column densities (NO_2 VCDs) with several semi-overlapping missions dating back to the 1990s [13–17]. In particular, the Ozone Monitoring Instrument (OMI) [16, 18] aboard the National Aeronautics and Space Administration (NASA) Aura satellite provides a daily global record of NO_2 columns since 2004, which

has been used extensively to infer the trends and sources of NO_x emissions from regional to global scales [10, 19].

Since the 1970s, the U.S. Environmental Protection Agency has prioritized policies and technologies to reduce NO_x emissions from the combustion of fossil fuels, resulting in an array of benefits for the nation's air quality [20]. In California, a number of techniques, including OMI satellite retrievals, have been used to examine the efficacy of statewide NO_x emission controls, although non-uniformly across the state [21]. The California Air Resources Board (CARB) emissions inventory reported a ∼43% reduction in anthropogenic NO_x emissions over the period of 2009–2020 ($-3.6\%a^{-1}$) [22]. Based on OMI satellite measurements, Lamsal *et al* [23] estimated comparable reductions from 2005 to 2013 in Southern California ($-5.2\%a^{-1}$) and the Central Valley ($-4.4\%a^{-1}$). Similarly, Russell *et al* [24] estimated reductions of OMI NO_2 columns ranging from -4.6 to $-5.7\%a^{-1}$ in California urban regions in the period from 2005–2011. These and other satellite studies across the US [10, 25–28] have found a marked discontinuity in rates of decline around 2009, reporting summertime trends in remote regions that flatten ($\sim 0\%a^{-1}$) [10] or even rise ($+2.0\%a^{-1}$) [24]. Most have proposed reasons for these recent trends to be related to the growing relative importance of 'natural' or uncontrolled NO_x sources like soil, lightning, and possibly wildfires. While many have assumed the abrupt change had to do with the economic downturn around 2009, Wang *et al* [27] use multivariate trend analysis to argue that just by meteorological chance the trends in the combined emissions from soils and lightning changed from $-4\%a^{-1}$ before 2009 to $+0.6\%a^{-1}$ afterwards.

Despite long-term progress, non-attainment of national air quality standards persists throughout California's Central Valley and other inland areas [29–31]. De Foy *et al* [32] reported that O_3 concentrations in the San Joaquin Valley (SJV) exceeded the National Ambient Air Quality Standards for ground-level O_3 (70 ppb) on 71 d in 2017 and 43 d in 2018. Similarly, Burley *et al* [33] found that the Sierra Nevada Mountains occasionally experience O_3 exceedances during the summer months with 5 d in 2013 and 16 d in 2014. As substantial reductions in anthropogenic NO_x emissions have been achieved, recent work has demonstrated that the O_3 formation regime has shifted to NO_x-limited in these non-attainment inland areas since the 2010s [32], and that O_3 formation has become more sensitive to perturbations in free tropospheric background NO_x attributed to biogenic emissions [10, 34]. For example, Sha *et al* [35] estimated that soil emissions account for 40.1% of California's total NO_x emissions for the month of July 2018, which significantly increase the surface NO_2 (+176.5%) and O_3 (+23.0%) concentrations in California. This finding is in agreement with other work that has identified soil NO_x emissions as an important component of the overall budget [9, 27, 36]. Moreover, Pan and Faloona [37] reported that O_3 levels are enhanced, on average, by 10% in California's Central Valley during wildfire-influenced periods, which were identified 1 in 5 d during June–September from 2016–2020. Although lightning is much less of an influence in California than in most of the rest of the US [7], previous studies have identified the role of both persistent and fugitive NO_x emissions over croplands and associated with wildfire smoke in the degradation of air quality in California's inland rural communities [29, 38, 39]. However, historical trend analyses of soil and wildfire NO_x emissions in California have been largely neglected, especially over the last decade as surface temperatures and biomass burning have increased markedly (figure S1).

Here we use satellite NO_2 columns from the OMI and a surface monitoring network to examine the temporal trends of NO_2 across five land cover types in California during the summer months (June–September) from 2009 to 2020. For non-urban regions where soil and wildfire emissions could be dominant NO_x sources, multiple gridded climate data sets are used along with a fire dataset to explore the influence of meteorological conditions and wildfires on the NO_2 levels and to make crude estimates of their growing importance by mid-century. Our study highlights the rise in wildfire and soil NO_x emissions in inland California over the past decade and may provide guidance for understanding future air quality in the region.

2. Materials and methods

2.1. California land cover classification

We use the Terra and Aqua combined Moderate Resolution Imaging Spectroradiometer (MODIS) Land Cover Type (MCD12Q1) Version 6 data product with a spatial resolution of 500 m to classify the land cover types across California [40]. In our trend analysis, we merge the MODIS land covers into five distinct types: urban, forests, croplands, scrublands, and barren based on the land cover distributions (figure S2(a)). The subordinate types within the forests or scrublands categories have similar NO_2 concentrations (difference $<0.16 \times 10^{15}$ molec cm^{-2}), annual NO_2 trends (difference $<1.8\%a^{-1}$), and responses to temperature and soil moisture (figure S2, table S1). The distribution of the five simplified land covers is shown in figure 1(a). Overall, California's land cover is primarily made up of scrublands (48.4%), forests (22.8%), and barren lands (15.3%). Agriculture is also an important land use in California, with the Central Valley being one of the most productive

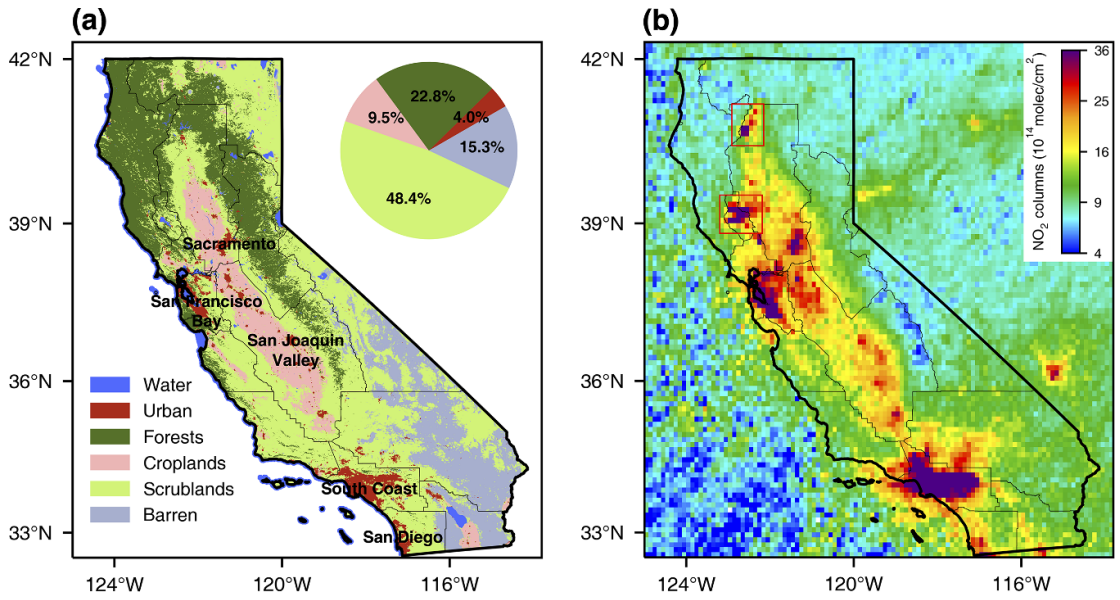

Figure 1. (a) Map of the MODIS land cover types across California. (b) June–September average TROPOMI NO_2 columns over California in 2018. The wildfire NO_2 hotspots are outlined in red rectangles. The borders within the maps represent the boundaries of the 15 air basins designated by CARB for regional management.

agricultural regions in the world, where nitrogen-rich fertilizers are applied to the vast cropland areas (9.5%) [36]. Urban areas account for a relatively small part (4.0%), mainly located in the state's coastal regions.

2.2. NO_2 column retrievals

The OMI measures backscattered solar radiation from the earth in the ultraviolet and visible wavelength range from 270 to 500 nm [16]. It provides daily global measurements of various trace gases, including NO_2 with a 2600 km wide swath and a spatial resolution of 13 × 24 km^2 for nadir pixels. We use three versions of OMI NO_2 column retrievals: the NASA NO_2 column retrieval [41], the Berkeley High-Resolution (BEHR) retrieval [42], and the Quality Assurance for Essential Climate Variables (QA4ECV) retrieval [43, 44]. The area-weighted average algorithm described by Jin *et al* [45] is used to grid the daily Level-2 swaths to the monthly mean NO_2 columns over California with a spatial resolution of 0.1° × 0.1°. To ensure the quality and stability of the satellite data, we select observations with cloud fraction <0.3, solar zenith angle <80°, surface albedo <0.3, and no 'row anomaly (RA)' data [46]. The pixels at the swath edge (first and last five rows) are also removed for QA4ECV and NASA retrievals.

The TROPOspheric Monitoring Instrument (TROPOMI) was launched by the European Space Agency (ESA) for the European Union's Copernicus Sentinel-5 Precursor (S5p) satellite mission in October 2017 [17]. TROPOMI samples daily at 13:30 local overpass time with an unprecedented horizontal resolution as fine as 3.5 × 5.5 km in nadir (3.5 × 7 km before August 2019). In order to compare with the OMI NO_2 columns, the daily TROPOMI Level-2 NO_2 columns during 2018–2020 are sampled to 0.1° × 0.1° with cloud fraction <0.3, solar zenith angle <80°, surface albedo <0.3, and the quality assurance value (qa) >0.75.

2.3. Surface NO_2 measurements

The surface NO_2 measurements during summer (June–September) from 2009 to 2020 are collected from the CARB. The hourly data are averaged over the afternoon hours (12:00–16:00) to temporally match the OMI measurements. There are 68 CARB NO_2 sites with continuous records between 2009 and 2020 which are selected to compare with the satellite data over five metropolitan air basins designated by CARB (South Coast, San Diego County, San Francisco Bay, SJV, and Sacramento County) as well as other, more remote regions. The distribution of measurement sites is shown in figure 2(a).

2.4. Meteorological datasets

To explore the meteorological effects on the NO_2 trends, we use the reanalysis data from the fifth-generation European Centre for Medium-Range Weather Forecasts (ERA5, ERA5-Land) [47, 48], Parameter-elevation Relationships on Independent Slopes Model (PRISM) climate group [49], and the NCEP North American Regional Reanalysis (NARR) [50]. The variables considered in this study include 2 m air temperature, soil moisture, precipitation, planetary boundary layer height, horizontal wind

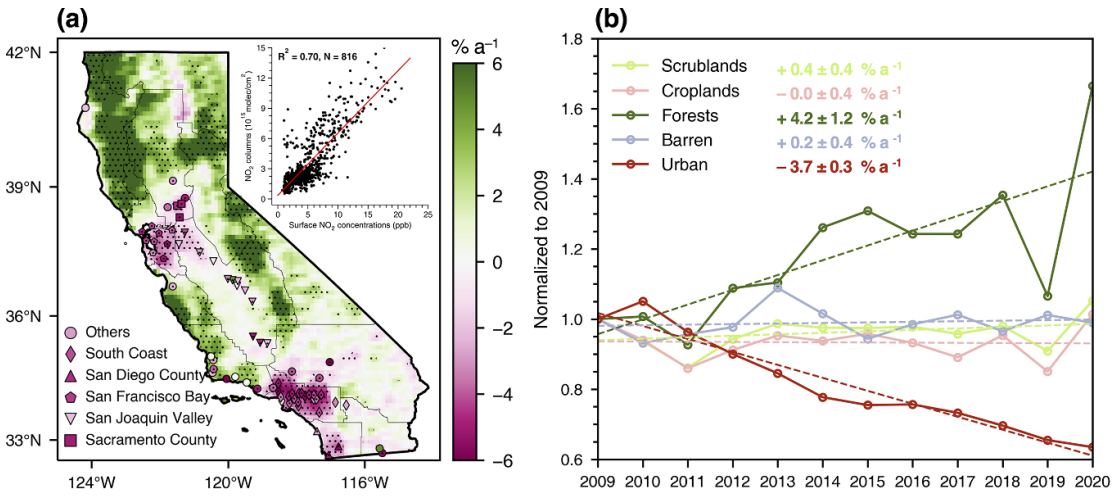

Figure 2. Trends (%a^{-1}) in June–September average NO_2 levels over California during 2009–2020. (a) Spatial distributions of the trends from QA4ECV OMI NO_2 columns and CARB ambient monitoring network with continuous annual records for 2009–2020. Statistically significant trends with p-values <0.05 are marked with black dots. The shade of color in the bottom left legend represents the average trends in %a^{-1} from the surface measurements for each region. The insert shows the June–September seasonal average NO_2 surface concentrations compared to VCDs from 2009 to 2020. R^2 represents the coefficient of determination and N is the number of data points in the scatter plot. (b) The NO_2 column trends are separated into urban, forests, croplands, scrublands, and barren lands defined by the land covers in figure 1(a). Ordinate values are ratios relative to 2009. The mean ± standard deviation annual percent change is shown in the inset.

speed, downward shortwave radiation, and cloud cover. The meteorological datasets used in this study are summarized in table S2.

2.5. Wildfire records

The California statewide database of fire history is obtained from the Fire and Resource Assessment Program (FRAP), which compiles fire perimeters from CAL FIRE, the United States Forest Service Region 5, the Bureau of Land Management, and the National Park Service. This data includes the California fire events that occurred since 1950 along with fire alarm dates, containment dates, area burned, and the causes of ignition. This work focused on the wildfire events that happened during the summer months (June–September) from 2009 to 2020, covering a total burned area of ∼7.8 million acres across 3117 separate fires.

2.6. Temperature/soil moisture dependence

For non-urban regions where the soils have been identified as a major source of NO_x emissions [9], the parameterization of Berkeley–Dalhousie soil NO_x emissions (BDSNP) [51], which is commonly used in chemistry transport models, is adopted to capture the relationship between meteorological variables and NO_2 columns. In the BDSNP scheme, soil NO_x emissions increase exponentially with temperature in the temperature-sensitive regime (0 °C–30 °C) and remain constant when the temperature is above 30 °C for wet soils [51, 52]. Similarly, an exponential function is fitted to the relationship between NO_2 columns and temperature in this study:

$$[NO_2](T) = \begin{cases} a \cdot \exp(b \cdot T) + c & T < T_0 \\ a \cdot \exp(b \cdot T_0) + c & T \geqslant T_0 \end{cases} \quad (1)$$

where $[NO_2]$ represents the NO_2 columns, T is the temperature (in degrees Celsius, only above freezing), T_0 is the upper limit of the temperature-sensitive regime. Unlike the BDSNP scheme which fixes T_0 to 30 °C for all wet soils, we customize different T_0 values across land types based on their observed temperature dependencies (discussed in section 3.3). First, the exponential function in equation (1) is fitted to the relationship between NO_2 VCDs and air temperature in all non-urban regions (the sum of forests, croplands, scrublands, and barren) (figure S9). Optimal values for the three parameters (a, b, and c) are calculated based on the fit. Parameter b is then assumed constant and applied to the fittings over all land types, with the optimal parameters a and c acquired for each land type. This procedure corresponds to what was done in the original study by Yienger and Levy [53], but allows us to determine these parameters independently.

The non-linear relationship between soil NO_x emissions and soil moisture is typically described by a Poisson function, with the lowest emissions at both extremely dry and wet conditions [51, 54]. A Poisson distribution is fit for the relationship between OMI NO_2 VCD and volumetric soil moisture (VSM) as

shown in equation (2), with the optimized parameters (a, b, and c) selected based on the same criteria as the temperature fittings. Where $[NO_2]$ represents the NO_2 VCD and θ is the VSM.

$$[NO_2](\theta) = a \cdot \theta \cdot \exp\left(-b \cdot \theta^2\right) + c \qquad (2)$$

Although T and θ are inversely correlated across the landscape (figure S6(b)), largely due to altitude, we make the fits to equations (1) and (2) independently to allow all six parameters to be solved for.

3. Results and discussion

3.1. Spatially heterogeneous NO_2 trends

Figure 2 and tables S1, S3, and S4 show the trends of summertime NO_2 concentrations during 2009–2020 in California from the Quality Assurance for Essential Climate Variables (QA4ECV) OMI retrievals [43] and ground measurements. We present here the summertime (June through September) trends because they are most relevant to persistent O_3 issues [29–32] and were found to have more pronounced flat or increasing trends than other seasons, and we begin our analysis in 2009 to avoid the discontinuity in trends found before that time [26]. Comparisons with trends detected using the NASA standard product, BEHR [42], and TROPOMI [55] retrievals (table S3 and figure S3) show excellent agreement. Continued, significant reductions in the NO_2 columns are observed in California's urban areas from 2009–2020 at a rate of $-3.7 \pm 0.3\%a^{-1}$, which is slightly smaller than the range (-3.9 to $-5.7\%a^{-1}$) of diminution reported in previous studies (table S4), but this difference is likely attributable to slower rates of change in the years subsequent to 2009 [26]. We further compared the OMI NO_2 column trends to surface NO_2 concentrations derived from the CARB air quality network. The afternoon (12:00–16:00) surface NO_2 concentrations are closely correlated ($R^2 = 0.70$, $N = 816$) with the NO_2 columns across the state (figure 2(a)). At the air basin scale over the South Coast, both the satellite ($-4.5 \pm 0.5\%a^{-1}$) and ground measurements ($-4.6 \pm 0.4\%a^{-1}$) demonstrate a coherent decline in NO_2 ($p < 0.05$) (figure S4). However, significantly slower rates of decline were found by satellite in the other urbanized air basins across California relative to the surface measurements (figure S4). This is consistent with the findings of Lamsal *et al* [23] in relatively lower NO_x environments, and the interested reader is referred to that work for a thorough discussion of possible reasons for discrepancies between surface and satellite trends.

By contrast, NO_2 columns outside of California's urban centers show either non-significant (unchanging) or positive trends from 2009 to 2020 (figure 2). In particular, forested areas, which have been much more frequently affected by wildfires over the past two decades [56], exhibit a strongly increasing trend ($+4.2 \pm 1.2\%a^{-1}$) of NO_2 columns. Much more muted trends are seen in scrublands ($+0.4 \pm 0.4\%a^{-1}$), and statistically non-significant changes are found in barren ($+0.2 \pm 0.4\%a^{-1}$) and cropland regions ($0.0 \pm 0.4\%a^{-1}$).

3.2. Anthropogenic effects

Given the short NO_x lifetime during summer [57], we infer that regulations targeting fossil fuel combustion within and near urban areas would have a more limited impact on NO_2 levels in more remote regions during the summer months. To examine this hypothesis, we compare the weekly cycle of NO_2 columns between different land types (figure S5). This analysis reveals that NO_2 columns on weekends (Sundays) is on average 42% (1.8×10^{15} molec cm^{-2}) lower than on weekdays (Tuesdays–Fridays) in urban areas because of the well-documented pattern of human activities [32, 58], consistent with the hypothesis. Non-urban areas do not present significant declines on weekends, with only small, detectable decreases found in croplands (-0.3×10^{15} molec cm^{-2}) and scrublands (-0.2×10^{15} molec cm^{-2}). It is important to note that the observed NO_2 cycles are not influenced by the wildfires and soil emissions because the weekend-weekday variations in the burned area and temperature are less than 0.2% (table S5). Since the weekend-weekday effects on the trends of NO_2 columns are minimal in the forests and barren lands, which tend to be the farthest from urban centers (figure 1), we assume that fossil fuel sources affect these two land types negligibly.

3.3. Soil emissions effects

Soil emissions, modulated by soil microbes, weather conditions, and reactive nitrogen (N) amounts, have been identified as a significant source of NO_x in California, particularly in warm agricultural regions (croplands) with high fertilizer applications [9, 36, 59]. Figure S6 shows temporal correlations between NO_2 columns and a set of potential drivers over non-urban areas in California. The temperature ($r = 0.81$) and soil moisture ($r = -0.70$), which are two major factors driving soil emissions, are highly correlated with the NO_2 columns, though the correlations vary regionally (figure S7). For example, Northern California, dominated by forests and scrublands, has the strongest positive correlations with temperature ($r > 0.8$) and is inversely correlated with soil moisture ($r < -0.6$), while opposite relationships are found in much of the southeastern barren areas. This deviation highlights the variability of NO_2 dependencies upon soil conditions, and a fine-scale analysis is critical for accurately quantifying the impacts of soil emission on long-term NO_2 trends in California.

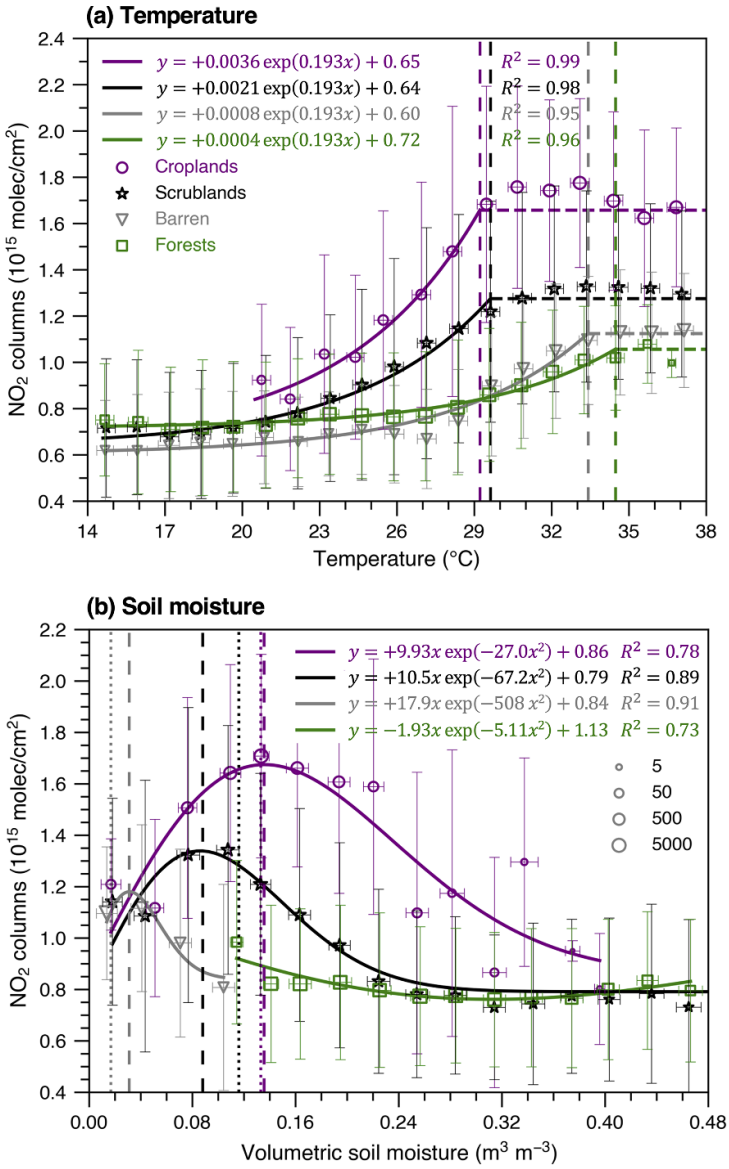

Figure 3. (a) Relationship between QA4ECV OMI NO_2 columns and ERA5-Land daily maximum temperature under different land covers. The solid lines are fitted exponential curves (equation (1)), and the vertical dashed lines represent the end of the temperature-sensitive regimes. (b) Relationship between NO_2 columns and ERA5-Land volumetric soil moisture (VSM). The solid lines are fitted Poisson curves (equation (2)). The vertical dashed lines indicate the maximum of the fitted curves, and vertical dotted lines show the median VSM of each land type. The scatter plots are binned by meteorological variables with standard deviation shown on each bin. The scatter points are sized based on the number of observations in each bin. R^2 represents the coefficient of determination.

Following the BDSNP [51], we apply a truncated exponential function (equation (1)) and a Poisson function (equation (2)) to depict the non-linear responses of NO_2 columns to temperature and VSM from the ERA5-Land reanalysis dataset (figures 3 and S8). High-fire months in the top 75th percentile of burned area (figure S9) and the highest 5% of NO_2 columns in each non-urban land type are excluded to eliminate the wildfire effects and remove any elevated NO_2 concentrations transported from urban centers [25] on rare occasions. The exponential function performed well in capturing the temperature dependence of NO_2 columns (figure 3, $R^2 > 0.95$), consistent with responses of soil NO_x emissions reported in previous studies [51–53]. We find that in croplands and scrublands our results agree with the BDSNP parameterization assuming a soil NO_x emission that increases exponentially followed by a plateau at 30 °C; however, in forests and barren lands we observe NO_2 columns reach their maxima at air temperatures closer to ~33 °C. This is possibly due to the difference in air vs. soil temperatures, but that effect would most likely work in differing directions during midday in summer over forests (cooler soils) than over non-vegetated lands (warmer soils). Another possibility for the difference could be microbial adaptations to

high temperatures or the importance of deep, cooler soil layers to the total NO_x emissions [9].

All land types tend to yield a very similar background concentration (parameter c in equation (1)) of $\sim 6.6 \pm 0.6 \times 10^{14}$ molec cm^{-2}, which is comparable to the values consistently observed well offshore by TROPOMI (figure 1(b)) [58] and OMI retrievals ($\sim 5.5 \pm 0.6 \times 10^{14}$ molec cm^{-2}), which moreover exhibit no significant trend during 2009–2020 (figure S10) [60]. Further, the pre-exponential factors (parameter a in equation (1)) in figure 3(a) are related in magnitude in a manner consistent with the 'wet' emission factors outlined in the original Yienger and Levy [53] parameterization with croplands being the largest (due to the higher available reactive N), scrublands (including open and closed shrublands, savannahs, and grasslands) are similar but smaller, and forests (including deciduous, evergreen, and mixed) an approximate order of magnitude smaller still. On the other hand, the larger temperature coefficients (parameter b in equation (1)) in our exponential fits indicate a much stronger temperature dependence than those of Yienger and Levy [53] and the other common parameterizations [35, 51] across all landscapes. After removing the background concentrations, the ratio of soil emissions for our data between 30 °C and 20 °C is a factor of 6.9 larger, whereas the traditional parameterizations predict an increase by a factor of 2.8. A recent study focusing on high-temperature agricultural soils over the US [27] proposed a stronger soil temperature dependence between 20 °C – 30 °C (a factor of 3.9 greater) and a higher threshold temperature at which emissions plateau (40 °C) relative to prevailing parameterizations. Both of these characteristics are qualitatively supported by our results across all landscapes in California illustrated in figure 3(a).

By controlling the ratio of oxygen to water in the soil pore space, soil moisture is another important factor regulating soil NO_x emissions [61]. Distinctly different VSM dependences of NO_2 columns are observed for the four non-urban land types (figure 3(b)), although they have similar patterns to the typical dependence of soil emission parameterizations [51, 61]. That is, the NO_2 columns are low in both extremely dry and wet conditions with the highest NO_2 columns observed at VSM values between 0.03–0.14, which can be accurately represented by the fit Poisson function ($R^2 > 0.73$). Many soil NO_x studies [35, 51, 62] use water-filled pore space (WFPS) to characterize soil moisture, which is equal to VSM divided by the soil porosity. Most soils in California have a porosity in the range of 0.4–0.6 [63] so our VSM peaks correspond to WFPS values in the approximate range of 0.05–0.35. A recent study by Huber *et al* [64] updated the BDSNP parameterization to fix the soil NO_x emission peaks at the observed median VSM for spring/summer. Figure 3(b) shows the June–September median values of VSM by the dotted lines indicating that they are fairly similar to our observed peaks (difference <0.03) for each land type in California.

Using the empirically fit relationships shown in figure 3, we calculate the trends of NO_2 columns that are driven by temperature and VSM changes to estimate how much of the observed trends can be ascribed to soil NO_x emissions (figure 4(a)). We use the sum of temperature and VSM-driven NO_2 column changes to represent the soil emission effects. The results reveal that soil emissions can explain about one-third of the OMI NO_2 trends over all non-urban areas but this ranges from nearly all in scrublands to less than 10% of the observed change in forested regions. This important environmental soil NO_x enhancement is dominated by the temperature-driven response, rather than the VSM-driven response, mostly because temperature has exhibited a more significant trend ($\sim +1.2$ °C $decade^{-1}$) than soil moisture ($\sim -1\%$ $decade^{-1}$) in the reanalysis data over the study period (figure S7). In particular, scrublands show the largest increase (0.48×10^{13} molec cm^{-2} a^{-1}), followed by forests (0.28×10^{13} molec cm^{-2} a^{-1}), and then croplands (0.17×10^{13} molec cm^{-2} a^{-1}), with barren areas indicating no net change from changing soil conditions because of the opposing temperature and VSM effects. As a reminder, in our fits we have only considered periods that are not substantially impacted by wildfire or urban emissions. Thus, the difference between the summed results and the observed trends likely indicates the changing influence of wildfires (discussed later) and urban emissions. It is worth noting that although the temperature dependence of NO_2 columns is strongest in croplands in the temperature range between 20 °C – 30 °C, the predicted soil emission change is small because of the assumed plateau above ~30 °C. This is because only 6.6% of the summertime temperatures over croplands fall below the threshold in the temperature-sensitive regime during OMI overpass time (~13:30 LT) (figure S11(a)), thereby muting the climate warming effects. Nearly half of all scrublands, on the other hand, appear to be at temperatures below its plateau temperature making their overall emissions much more susceptible to rising temperatures (figure S11(b)). Because of their higher average temperature plateau threshold and elevations, forest soils are mostly all susceptible to increasing temperatures even though their absolute emissions are smaller than those in croplands and scrublands.

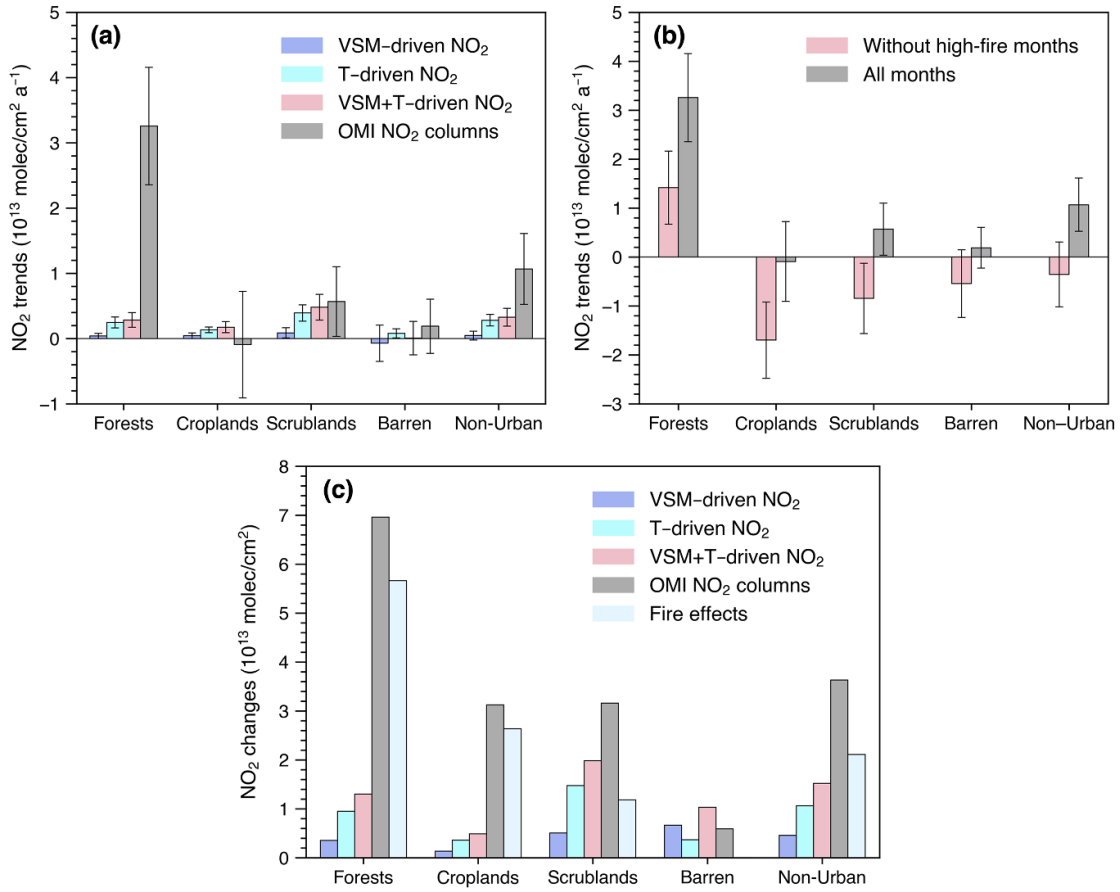

Figure 4. (a) Trends of June–September average QA4ECV OMI NO_2 columns and the components driven by temperature and soil moisture changes across forests, croplands, scrublands, barren, and total non-urban areas of California during 2009–2020. (b) Trends of the QA4ECV OMI NO_2 columns for all months and those without the high-fire (upper quartile) months. The error bars show the standard deviation of the trends. (c) Changes in average QA4ECV OMI NO_2 columns and temperature/soil moisture-driven NO_2 columns between all months and those without high-fire months during June–September from 2009 to 2020. The estimated fire effects are calculated as the differences between the total OMI NO_2 columns and the estimated soil changes (VSM + T-driven NO_2).

3.4. Wildfire effects

A recent study of the background NO_2 in the US revealed that soil emissions, lightning, and meteorological changes simulated by the GEOS-Chem model could not fully explain the observed decadal rise in remote NO_2 during summer [28] and further suggested that deficiencies in the model's treatment of wildfire NO_x could be the culprit. Another study by Wang *et al* [27] suggested that the abrupt deceleration in NO_x reductions observed in 2009 was due to a coincident change in the soil and lightning emissions at that time, conceding that wildfire emissions while rising rapidly ($\sim$6.5%a^{-1}) were still too small of a source to influence total NO_x trends accounting for only 1.9% of the US inventory in the period from 2005–2019. Although this work and a number of other studies have demonstrated an underestimation of soil NO_x emissions [9, 27, 35, 36] in current models, we further infer that the dramatically increasing biomass burning activity over the past two decades [56], in California in particular, is a critical factor contributing to a dramatic shift in background NO_2 trends. Figure 4(b) shows the differences in trends of NO_2 columns after removing the upper 75th percentile wildfire-impacted months as measured by statewide area burned (figure S9). This upper quartile threshold was selected because there were months in this range distributed across most of the study period (figure S9). Statistically significant decreased rates are observed in all urban (-2.1×10^{13} molec cm^{-2} a^{-1} reducing the trend from -3.7 to -4.2%a^{-1}) and non-urban land cover types (figure 4(b)), with the most pronounced declines found in forests (-1.8×10^{13} molec cm^{-2} a^{-1}), followed by croplands (-1.6×10^{13} molec cm^{-2} a^{-1}) and scrublands (-1.4×10^{13} molec cm^{-2} a^{-1}), and a relatively minor impact in barren regions (-0.7×10^{13} molec cm^{-2} a^{-1}). Our results further reveal that the offshore, background NO_2 column trends are not affected by wildfires (figures S10(b) and (c)). Considering that the warmer and drier conditions during high-fire months may also enhance the soil NO_x emissions, we further compare the predicted temperature and VSM-driven NO_2 changes

Table 1. Predictions of June–September average NO_2 changes driven by soil moisture, temperature, and wildfires in California forests and barren lands during 2009–2020, and 2020–2050 (10^{13} molec cm^{-2}).

Period	Soil moisture	Temperature	Wildfires	OMI/Total
Forests				
2009–2020	$+0.4 \pm 0.4$	$+2.7 \pm 0.9$	$+32.7 \pm 9.3$	$+35.8 \pm 9.9$ (+46.3%)
2020–2050	+1.2	+7.3	+415.5	+424.0 (+329.6%)
Barren				
2009–2020	-0.8 ± 3.1	$+0.9 \pm 0.8$	$+2.0 \pm 5.6$	$+2.1 \pm 4.6$ (+2.7%)
2020–2050	−2.2	+2.3	+25.4	+25.5 (+22.5%)

with the OMI NO_2 columns to isolate the influences from wildfires and soil emissions (figure 4(c)). Our results reveal that these two factors have comparable influences on the NO_2 columns across the entirety of non-urban regions, although their contributions varied significantly in different land covers. For example, the NO_2 columns in croplands and scrublands show similar enhancements, with wildfires being the major contributors (84%) in croplands, while soil emissions have a greater impact on scrublands (63%).

Recall from figure S5 that the fossil fuel effects are minimal in the remote forest and barren regions, and so we estimate the effects of wildfires on the NO_2 trends in these two surface types by subtracting the influence of temperature and soil moisture from the OMI NO_2 columns. The difference is not an exact quantification however because we are only able to eliminate some arbitrary top percentile (in this case the 75th) of wildfire impacts. The results nevertheless show that the substantial rise in summertime NO_2 concentrations in forest habitats is mostly driven by increasing wildfire emissions, accounting for ∼90% of the OMI NO_2 trend (figure 4(a)). One can also discern this effect in the observations of greater mean VCDs across the Northern California mountains and the Central Sierra Nevada in the summertime relative to the wintertime despite the much shorter photochemical lifetime (figure S12). This hypothesis is further supported by the fact that the NO_2 columns in forest regions show a much weaker trend ($0.4 \pm 0.8 \times 10^{13}$ molec cm^{-2} a^{-1}) during the winter months (December–March) when the NO_2 columns are not significantly affected by the wildfires (figure S13). For barren lands, wildfire is also the major driver of their moderately increasing trends.

4. Future implications

Figure S14 graphically demonstrates the increase in California burned areas which can be represented by an exponential function since the 1970s ($R^2 = 0.32$) [65] with a doubling time scale of about a decade. Given the linear responses of NO_2 columns to burned areas ($R^2 = 0.14$, figure S15) [66], and the NO_2 trends driven by temperature and VSM as shown in figure 4(a), we crudely predict the approximate NO_2 changes in 2050 for the remote forests and barren regions by simply extrapolating these wildfire and soil emission effects (table 1). Our results indicate that the NO_2 columns in the forests could be more than four times larger than current levels in 2050 if the fire activities continue to increase in the coming decades as expected in California [65]. However, there are many feedbacks that remain highly uncertain such as the accumulation of N in soils as wildfire emissions continue to rise leading to soil microbial changes and lag effects that may further influence future soil emissions. In any event, significant rises in background NO_2 will likely resist the continuation of gains from fossil fuel NO_x controls and represent a growing challenge for future air quality management across the state and potentially across the entire western US.

5. Conclusions

Using long-term (2009–2020) observations from the OMI satellite measurements, this study depicts spatial patterns in summertime NO_2 trends across California. Our results reveal a significant NO_2 improvement within cities, while the non-urban regions show either no detectable changes or steadily increasing NO_2 columns (in forested regions). We then quantitatively evaluate the impacts of the major NO_x sources, focusing on three main sources: fossil fuel emissions, soil emissions, and wildfire emissions. In general, the rising soil and wildfire emissions combined are offsetting the anthropogenic NO_x decline over non-urban portions of the state, and the wildfires play a more important role in determining the trends of NO_2 columns than do the soil emissions, although the relative contributions of these two sources vary a lot in distinct land types. With continued progress in regulating fossil fuel NO_x emissions, these less-understood NO_x sources will become increasingly important to air quality control strategies in California. Our results point to opportunities for different sets of policies and technologies to assist in reducing NO_2 concentrations in rural and economically disadvantaged areas of California, but will require a concerted effort to better understand the

exact environmental dependence of soil and wildfire emissions.

Data availability statements

The data that support the findings of this study are openly available at the following URL/ DOI: MODIS land cover type data are available at https://doi.org/10.5067/MODIS/MCD12Q1.006. Surface NO_2 concentrations are downloaded from the CARB (www.arb.ca.gov/aqmis2/aqmis2.php). OMI NO_2 columns are derived from QA4ECV (www.qa4ecv.eu/), NASA (https://doi.org/10.5067/Aura/OMI/DATA2017), and BEHR (http://behr.cchem.berkeley.edu) retrievals. The TROPOMI NO_2 columns are downloaded from NASA GES DISC (https://disc.gsfc.nasa.gov). The monthly climate data are extracted from PRISM (https://prism.oregonstate.edu) and NARR (https://psl.noaa.gov/data/gridded/data.narr.html). The ERA5 and ERA5-Land hourly reanalysis data are available from the Copernicus Climate Service (C3S) Climate Data Store (https://climate.copernicus.eu). The wildfire records are obtained from FRAP (https://frap.fire.ca.gov/frap-projects/fire-perimeters/).

Acknowledgments

I C Faloona's effort was supported by the USDA National Institute of Food and Agriculture, [Hatch Project CA-D-LAW-2481-H, 'Understanding Background Atmospheric Composition, Regional Emissions, and Transport Patterns Across California']. The authors are also grateful to F Boersma for helping us with quality assurance of the different satellite data sets, and we would like to thank D D Parrish, C D Cappa, and M Kleeman for a series of fruitful discussions regarding this work. We thank A T O'Geen for help interpreting the soil properties found in his California soil resource lab's SoilWeb database. The inputs of two anonymous reviewers also helped to improve the manuscript.

ORCID iDs

Yurun Wang https://orcid.org/0000-0003-4536-2227
Ian C Faloona https://orcid.org/0000-0001-7296-9046
Benjamin Z Houlton https://orcid.org/0000-0002-1414-0261

References

[1] Caiazzo F, Ashok A, Waitz I A, Yim S H L and Barrett S R H 2013 Air pollution and early deaths in the United States. Part I: quantifying the impact of major sectors in 2005 *Atmos. Environ.* **79** 198–208
[2] Cohen A J *et al* 2017 Estimates and 25-year trends of the global burden of disease attributable to ambient air pollution: an analysis of data from the Global Burden Of Diseases Study 2015 *Lancet* **389** 1907–18
[3] Meng Y-Y, Rull R P, Wilhelm M, Lombardi C, Balmes J and Ritz B 2010 Outdoor air pollution and uncontrolled asthma in the San Joaquin Valley, California *J. Epidemiol. Community Health* **64** 142
[4] Sampedro J, Waldhoff S T, Van de Ven D-J, Pardo G, Van Dingenen R, Arto I, Del Prado A and Sanz M J 2020 Future impacts of ozone driven damages on agricultural systems *Atmos. Environ.* **231** 117538
[5] Tan Y, Henderick P, Yoon S, Herner J, Montes T, Boriboonsomsin K, Johnson K, Scora G, Sandez D and Durbin T D 2019 On-board sensor-based NO_x emissions from heavy-duty diesel vehicles *Environ. Sci. Technol.* **53** 5504–11
[6] de Foy B, Lu Z, Streets D G, Lamsal L N and Duncan B N 2015 Estimates of power plant NO_x emissions and lifetimes from OMI NO_2 satellite retrievals *Atmos. Environ.* **116** 1–11
[7] Schumann U and Huntrieser H 2007 The global lightning-induced nitrogen oxides source *Atmos. Chem. Phys.* **7** 3823–907
[8] Campbell P C, Tong D, Saylor R, Li Y, Ma S, Zhang X, Kondragunta S and Li F 2022 Pronounced increases in nitrogen emissions and deposition due to the historic 2020 wildfires in the western U.S *Sci. Total Environ.* **839** 156130
[9] Oikawa P Y, Ge C, Wang J, Eberwein J R, Liang L L, Allsman L A, Grantz D A and Jenerette G D 2015 Unusually high soil nitrogen oxide emissions influence air quality in a high-temperature agricultural region *Nat. Commun.* **6** 8753
[10] Silvern R F *et al* 2019 Using satellite observations of tropospheric NO_2 columns to infer long-term trends in US NO_x emissions: the importance of accounting for the free tropospheric NO_2 background *Atmos. Chem. Phys.* **19** 8863–78
[11] Laughner J L and Cohen R C 2019 Direct observation of changing NO_x lifetime in North American cities *Science* **366** 723–7
[12] Vandaele A C, Hermans C, Simon P C, Carleer M, Colin R, Fally S, Mérienne M F, Jenouvrier A and Coquart B 1998 Measurements of the NO_2 absorption cross-section from 42 000 cm^{-1} to 10 000 cm^{-1} (238–1000 nm) at 220 K and 294 K *J. Quant. Spectrosc. Radiat. Transfer* **59** 171–84
[13] Burrows J P *et al* 1999 The Global Ozone Monitoring Experiment (GOME): mission concept and first scientific results *J. Atmos. Sci.* **56** 151–75
[14] Bovensmann H, Burrows J P, Buchwitz M, Frerick J, Noël S, Rozanov V V, Chance K V and Goede A P H 1999 SCIAMACHY: mission objectives and measurement modes *J. Atmos. Sci.* **56** 127–50
[15] Callies J, Corpaccioli E, Eisinger M, Hahne A and Lefebvre A 2000 GOME-2-Metop's second-generation sensor for operational ozone monitoring *ESA Bull.* **102** 28–36 (available at: www.esa.int/esapub/bulletin/bullet102/Callies102.pdf)
[16] Levelt P F, Hilsenrath E, Leppelmeier G W, van den Oord G H J, Bhartia P K, Tamminen J, de Haan J F and Veefkind J P 2006 Science objectives of the ozone monitoring instrument *IEEE Trans. Geosci. Remote Sens.* **44** 1199–208
[17] Veefkind J P *et al* 2012 TROPOMI on the ESA Sentinel-5 Precursor: a GMES mission for global observations of the atmospheric composition for climate, air quality and ozone layer applications *Remote Sens. Environ.* **120** 70–83
[18] Levelt P F *et al* 2018 The ozone monitoring instrument: overview of 14 years in space *Atmos. Chem. Phys.* **18** 5699–745
[19] Vinken G C M, Boersma K F, Maasakkers J D, Adon M and Martin R V 2014 Worldwide biogenic soil NO_x emissions inferred from OMI NO_2 observations *Atmos. Chem. Phys.* **14** 10363–81
[20] US EPA *Nitrogen Dioxide (NO2) Primary Air Quality Standards* (available at: www.epa.gov/naaqs/nitrogen-dioxide-no2-primary-air-quality-standards) (Accessed 1 August 2023)

[21] Russell A R, Valin L C, Bucsela E J, Wenig M O and Cohen R C 2010 Space-based constraints on spatial and temporal patterns of NO_x emissions in California, 2005-2008 *Environ. Sci. Technol.* **44** 3608–15
[22] CARB Criteria pollutant emission inventory data (available at: https://ww2.arb.ca.gov/criteria-pollutant-emission-inventory-data) (Accessed 1 August 2023)
[23] Lamsal L N, Duncan B N, Yoshida Y, Krotkov N A, Pickering K E, Streets D G and Lu Z 2015 U.S. NO_2 trends (2005–2013): EPA air quality system (AQS) data versus improved observations from the ozone monitoring instrument (OMI) *Atmos. Environ.* **110** 130–43
[24] Russell A R, Valin L C and Cohen R C 2012 Trends in OMI NO_2 observations over the United States: effects of emission control technology and the economic recession *Atmos. Chem. Phys.* **12** 12197–209
[25] Lu Z, Streets D G, de Foy B, Lamsal L N, Duncan B N and Xing J 2015 Emissions of nitrogen oxides from US urban areas: estimation from ozone monitoring instrument retrievals for 2005–2014 *Atmos. Chem. Phys.* **15** 10367–83
[26] Jiang Z *et al* 2018 Unexpected slowdown of US pollutant emission reduction in the past decade *Proc. Natl Acad. Sci. USA* **115** 5099–104
[27] Wang Y, Ge C, Castro Garcia L, Jenerette G D, Oikawa P Y and Wang J 2021 Improved modelling of soil NO_x emissions in a high temperature agricultural region: role of background emissions on NO_2 trend over the US *Environ. Res. Lett.* **16** 084061
[28] Qu Z, Jacob D J, Silvern R F, Shah V, Campbell P C, Valin L C and Murray L T 2021 US COVID-19 shutdown demonstrates importance of background NO_2 in inferring NO_x emissions from satellite NO_2 observations *Geophys. Res. Lett.* **48** e2021GL092783
[29] Parrish D D, Young L M, Newman M H, Aikin K C and Ryerson T B 2017 Ozone design values in Southern California's Air Basins: temporal evolution and U.S. background contribution *J. Geophys. Res. Atmos.* **122** 11,166–82
[30] Buysse C E, Munyan J A, Bailey C A, Kotsakis A, Sagona J A, Esperanza A and Pusede S E 2018 On the effect of upwind emission controls on ozone in Sequoia National Park *Atmos. Chem. Phys.* **18** 17061–76
[31] Trousdell J F, Caputi D, Smoot J, Conley S A and Faloona I C 2019 Photochemical production of ozone and emissions of NO_x and CH4 in the San Joaquin Valley *Atmos. Chem. Phys.* **19** 10697–716
[32] de Foy B, Brune W H and Schauer J J 2020 Changes in ozone photochemical regime in Fresno, California from 1994 to 2018 deduced from changes in the weekend effect *Environ. Pollut.* **263** 114380
[33] Burley J D *et al* 2016 Air quality at Devils Postpile National Monument, Sierra Nevada Mountains, California, USA *Aerosol Air Qual. Res.* **16** 2315–32
[34] Geddes J A, Pusede S E and Wong A Y H 2022 Changes in the relative importance of biogenic isoprene and soil NO_x emissions on ozone concentrations in nonattainment areas of the United States *JGR Atmos.* **127** e2021JD036361
[35] Sha T, Ma X, Zhang H, Janechek N, Wang Y, Wang Y, Castro García L, Jenerette G D and Wang J 2021 Impacts of soil NO_x emission on O_3 air quality in rural California *Environ. Sci. Technol.* **55** 7113–22
[36] Almaraz M, Bai E, Wang C, Trousdell J, Conley S, Faloona I and Houlton B Z 2018 Agriculture is a major source of NO_x pollution in California *Sci. Adv.* **4** eaao3477
[37] Pan K and Faloona I C 2022 The impacts of wildfires on ozone production and boundary layer dynamics in California's Central Valley *Atmos. Chem. Phys.* **22** 9681–702
[38] Parrish D D, Faloona I C and Derwent R G 2022 Observational-based assessment of contributions to maximum ozone concentrations in the western United States *J. Air Waste Manage. Assoc.* **72** 434–54
[39] Ninneman M and Jaffe D A 2021 The impact of wildfire smoke on ozone production in an urban area: insights from field observations and photochemical box modeling *Atmos. Environ.* **267** 118764
[40] Friedl M and Sulla-Menashe D 2019 MCD12Q1 MODIS/terra+aqua land cover type yearly L3 global 500m SIN grid V006 (https://doi.org/10.5067/MODIS/MCD12Q1.006)
[41] Krotkov N A and Veefkind P 2012 OMI/Aura nitrogen dioxide (NO_2) total and tropospheric column 1-orbit L2 swath 13x24 km (https://doi.org/10.5067/AURA/OMI/DATA2017)
[42] Russell A R, Perring A E, Valin L C, Bucsela E J, Browne E C, Wooldridge P J and Cohen R C 2011 A high spatial resolution retrieval of NO_2 column densities from OMI: method and evaluation *Atmos. Chem. Phys.* **11** 8543–54
[43] Boersma K F, Eskes H, Richter A, De Smedt I, Lorente A, Beirle S, Van Geffen J, Peters E, Van Roozendael M and Wagner T 2017 (Royal Netherlands Meteorological Institute (KNMI)) (https://doi.org/10.21944/qa4ecv-no2-omi-v1.1)
[44] Boersma K F *et al* 2018 Improving algorithms and uncertainty estimates for satellite NO_2 retrievals: results from the quality assurance for the essential climate variables (QA4ECV) project *Atmos. Meas. Tech.* **11** 6651–78
[45] Jin X, Fiore A, Boersma K F, Smedt I D and Valin L 2020 Inferring changes in summertime surface ozone–NO_x–VOC chemistry over U.S. urban areas from two decades of satellite and ground-based observations *Environ. Sci. Technol.* **54** 6518–29
[46] Schenkeveld V M E, Jaross G, Marchenko S, Haffner D, Kleipool Q L, Rozemeijer N C, Veefkind J P and Levelt P F 2017 In-flight performance of the ozone monitoring instrument *Atmos. Meas. Tech.* **10** 1957–86
[47] Hersbach H *et al* 2020 The ERA5 global reanalysis *Q. J. R. Meteorol. Soc.* **146** 1999–2049
[48] Muñoz-Sabater J *et al* 2021 ERA5-Land: a state-of-the-art global reanalysis dataset for land applications *Earth Syst. Sci. Data* **13** 4349–83
[49] Daly C, Halbleib M, Smith J I, Gibson W P, Doggett M K, Taylor G H, Curtis J and Pasteris P P 2008 Physiographically sensitive mapping of climatological temperature and precipitation across the conterminous United States *Int. J. Climatol.* **28** 2031–64
[50] Mesinger F *et al* 2004 North American regional reanalysis *Bull. Am. Meteorol. Soc.* **87** 343–60
[51] Hudman R C, Moore N E, Mebust A K, Martin R V, Russell A R, Valin L C and Cohen R C 2012 Steps towards a mechanistic model of global soil nitric oxide emissions: implementation and space based-constraints *Atmos. Chem. Phys.* **12** 7779–95
[52] Steinkamp J and Lawrence M G 2011 Improvement and evaluation of simulated global biogenic soil NO emissions in an AC-GCM *Atmos. Chem. Phys.* **11** 6063–82
[53] Yienger J J and Levy H 1995 Empirical model of global soil-biogenic NO_x emission *J. Geophys. Res.* **100** 11447
[54] van Dijk S M 2002 Biogenic NO emissions from forest and pasture soils: relating laboratory studies to field measurements *J. Geophys. Res.* **107** 8058
[55] van Geffen J H G M, Eskes H J, Boersma K F, Maasakkers J D and Veefkind J P 2019 TROPOMI ATBD of the total and tropospheric NO_2 data products (Royal Netherlands Meteorological Institute) (available at: https://sentinel.esa.int/documents/247904/2476257/sentinel-5p-tropomi-atbd-no2-data-products)
[56] Li S and Banerjee T 2021 Spatial and temporal pattern of wildfires in California from 2000 to 2019 *Sci. Rep.* **11** 8779
[57] Beirle S, Boersma K F, Platt U, Lawrence M G and Wagner T 2011 Megacity emissions and lifetimes of nitrogen oxides probed from space *Science* **333** 1737–9
[58] Goldberg D L, Anenberg S C, Kerr G H, Mohegh A, Lu Z and Streets D G 2021 TROPOMI NO_2 in the United States: a detailed look at the annual averages, weekly cycles, effects of temperature, and correlation with surface NO_2 concentrations *Earth's Future* **9** e2020EF001665

[59] Byrnes D K, Van Meter K J and Basu N B 2020 Long-term shifts in U.S. nitrogen sources and sinks revealed by the new TREND-nitrogen data set (1930–2017) *Glob. Biogeochem. Cycles* **34** e2020GB006626
[60] de Foy B, Lu Z and Streets D G 2016 Impacts of control strategies, the great recession and weekday variations on NO_2 columns above North American cities *Atmos. Environ.* **138** 74–86
[61] Pilegaard K 2013 Processes regulating nitric oxide emissions from soils *Phil. Trans. R. Soc.* B **368** 20130126
[62] Rasool Q Z, Zhang R, Lash B, Cohan D S, Cooter E J, Bash J O and Lamsal L N 2016 Enhanced representation of soil NO emissions in the community multiscale air quality (CMAQ) model version 5.0.2 *Geosci. Model Dev.* **9** 3177–97
[63] Walkinshaw M, O'Geen A T and Beaudette D E Soil Properties (California Soil Resource Lab) (available at: http://casoilresource.lawr.ucdavis.edu/soil-properties/) (Accessed 1 August 2023)
[64] Huber D E, Steiner A L and Kort E A 2023 Sensitivity of modeled soil NO_x emissions to soil moisture *JGR Atmos.* **128** e2022JD037611
[65] Abatzoglou J T and Williams A P 2016 Impact of anthropogenic climate change on wildfire across western US forests *Proc. Natl Acad. Sci. USA* **113** 11770–5
[66] Mebust A K, Russell A R, Hudman R C, Valin L C and Cohen R C 2011 Characterization of wildfire NO_x emissions using MODIS fire radiative power and OMI tropospheric NO_2 columns *Atmos. Chem. Phys.* **11** 5839–51